Supporting information for:

Enhanced photocatalytic activity of novel brown $H_4Nb_6O_{17}$/g-C_3N_4 composite for visible-light driven H_2O_2 production

Luona Zhang[a], Shiqi Zhao[a], Xiaorong Cheng[b], Zijie Liu[a], Ruochen Liu[a], Graham Dawson[a*]

[a]Department of Chemistry, Xi'an Jiaotong Liverpool University, Suzhou, Jiangsu, 215123, P. R. China

[b]Suzhou Vocational Institute of Industrial Technology, Suzhou, Jiangsu, 215104, P. R. China

* Corresponding author: graham.dawson@xjtlu.edu.cn

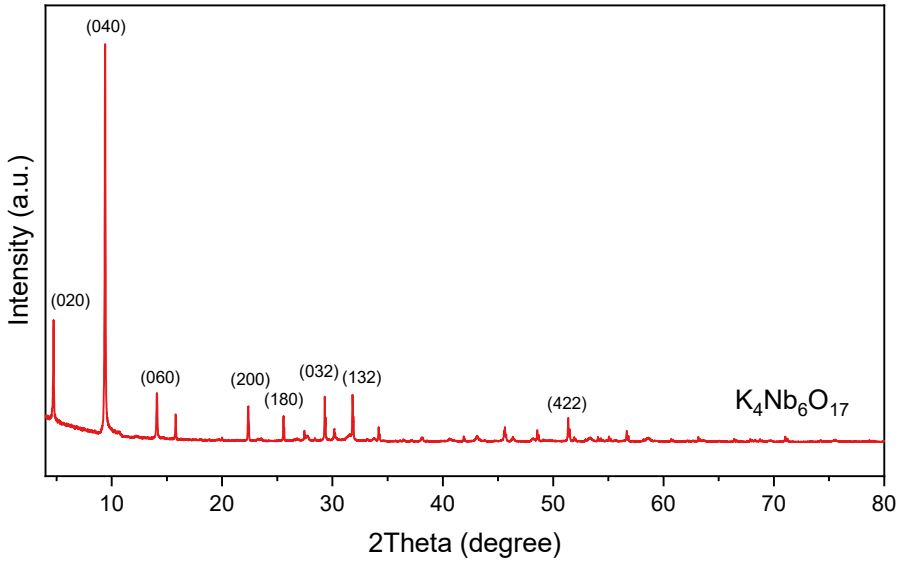

Figure S1. XRD pattern of as prepared $K_4Nb_6O_{17}$ indexed to JCPDS, No. 76-0977.

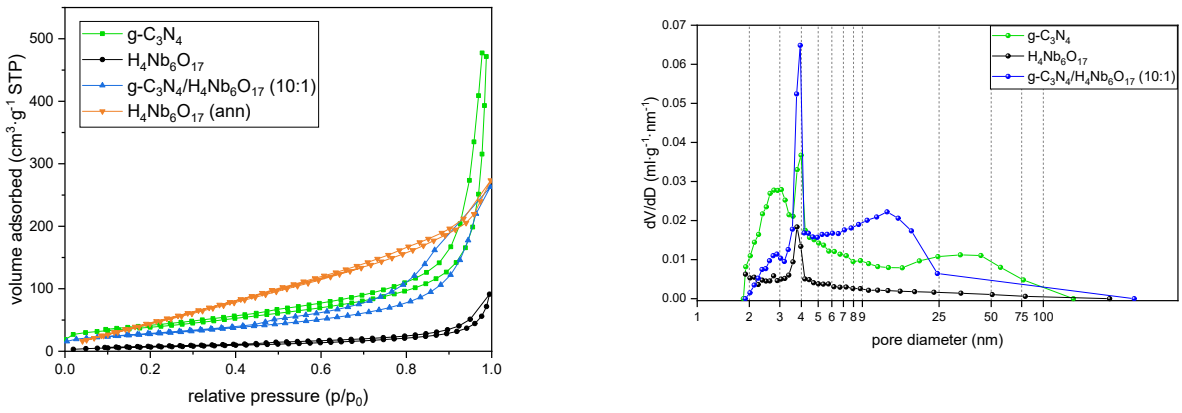

Figure S2. N_2 adsorption-desorption isotherms and BJH pore size distribution of the samples.

Table 1: BET surface areas and pore volume of the samples.

Sample	S_{BET} (m^2/g)	Pore volume (cm^3/g)
$H_4Nb_6O_{17}$	26.0	0.15
g-C_3N_4	139.0	0.89
$H_4Nb_6O_{17}$ (ann.)	104	0.43
g-C_3N_4/$H_4Nb_6O_{17}$ (10:1)	100.4	0.44

Figure S3. Zeta potential measurement for $H_4Nb_6O_{17}$ (ann) and g-C_3N_4.

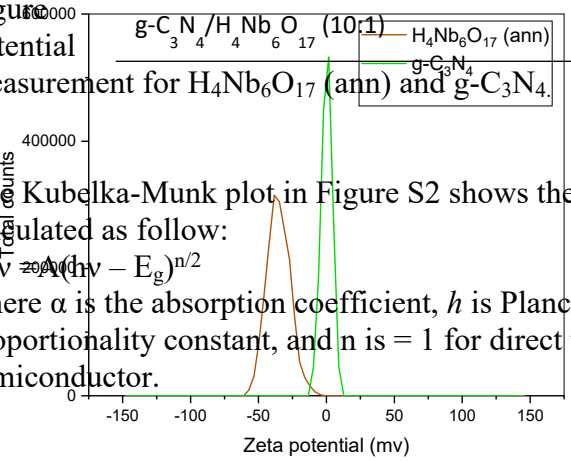

The Kubelka-Munk plot in Figure S2 shows the X axis band gap energy, E_g, and Y axis $(\alpha h\nu)^2$, calculated as follow:

$\alpha h\nu = A(h\nu - E_g)^{n/2}$

where α is the absorption coefficient, *h* is Planck's constant, ν is the photon energy, A is a proportionality constant, and n is = 1 for direct transition and =4 for indirect transition of the semiconductor.

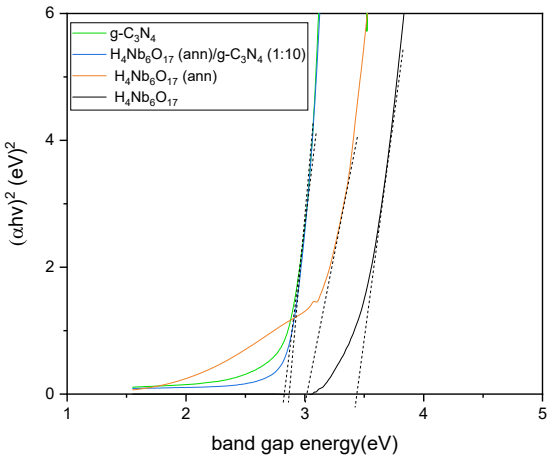

Figure S4. Kubelka-Munk plot of the samples calculated from the UV-vis data shown in Figure 4.

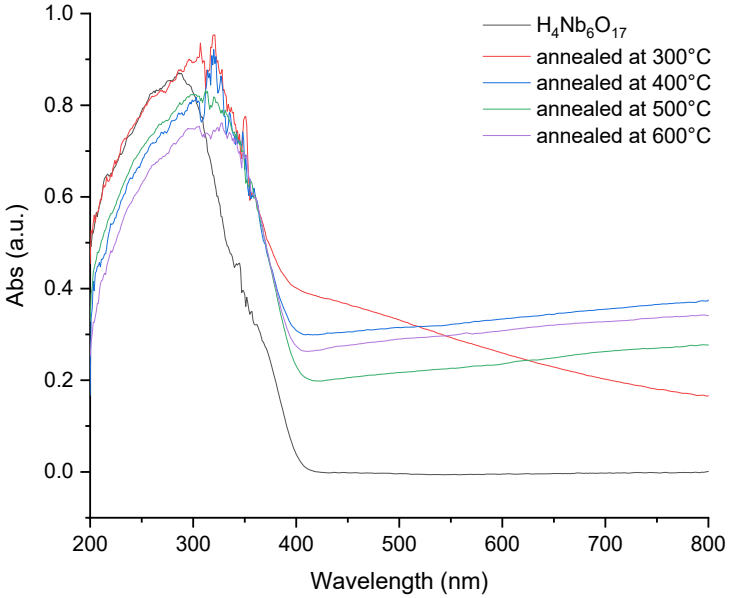

.

Figure S5. UV-vis spectra of $H_4Nb_6O_{17}$ annealed at different temperatures

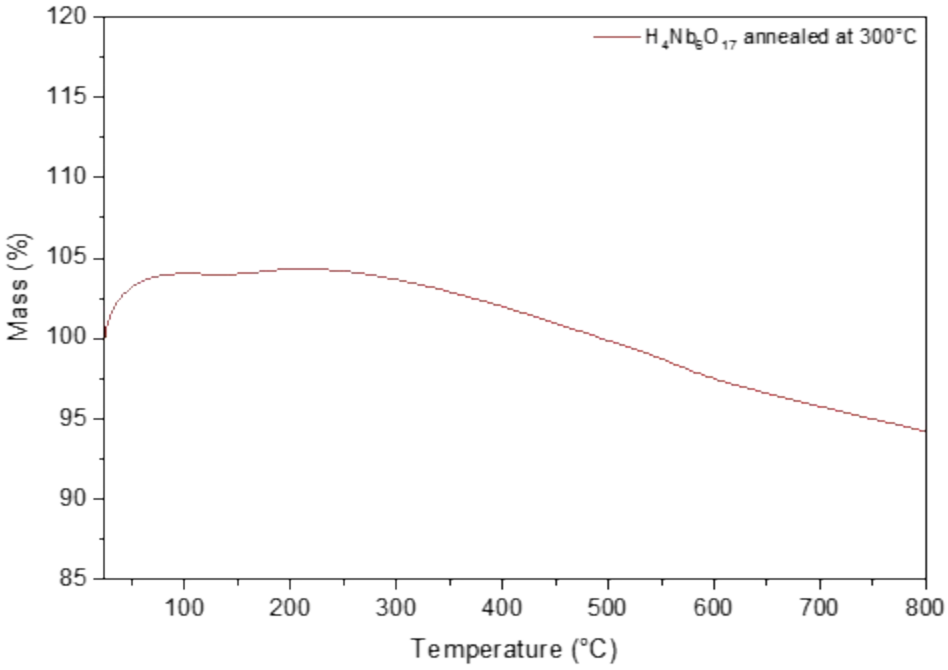

Figure S6. TGA of $H_4Nb_6O_{17}$ (ann)

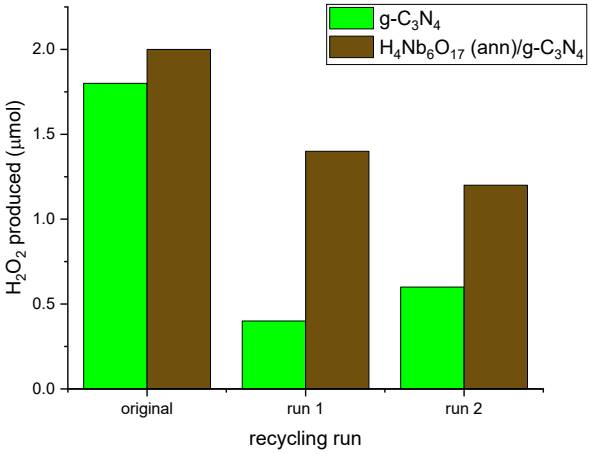

Figure S7. . Recycling ability for H_2O_2 production for g-C_3N_4 and $H_4Nb_6O_{17}$ (ann)/ g-C_3N_4 composite

Sample shows a mass loss between 250 and 570 ºC of ~7%, which can be ascribed to loss of incorporated organic material. Above this inflexion point decomposition is observed.

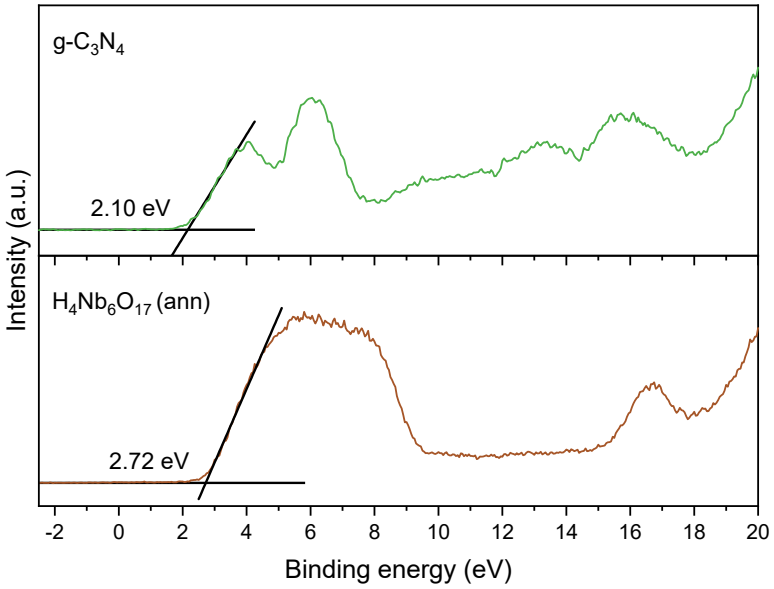

Figure S8. VB-XPS spectra of g-C_3N_4 and the annealed $H_4Nb_6O_{17}$.

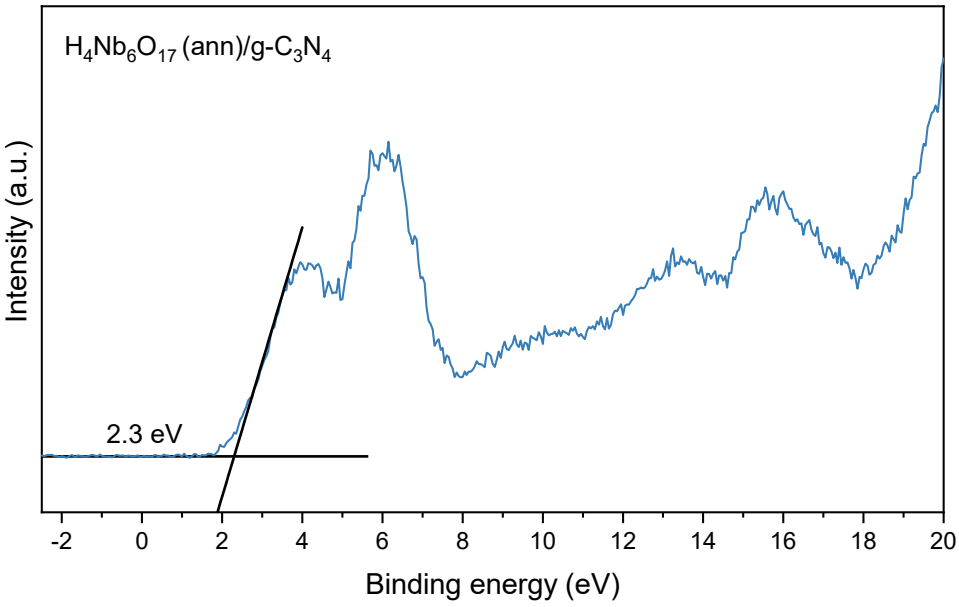

Figure S9. VB-XPS spectra of VB-XPS of $H_4Nb_6O_{17}$ (ann)/ g-C_3N_4.

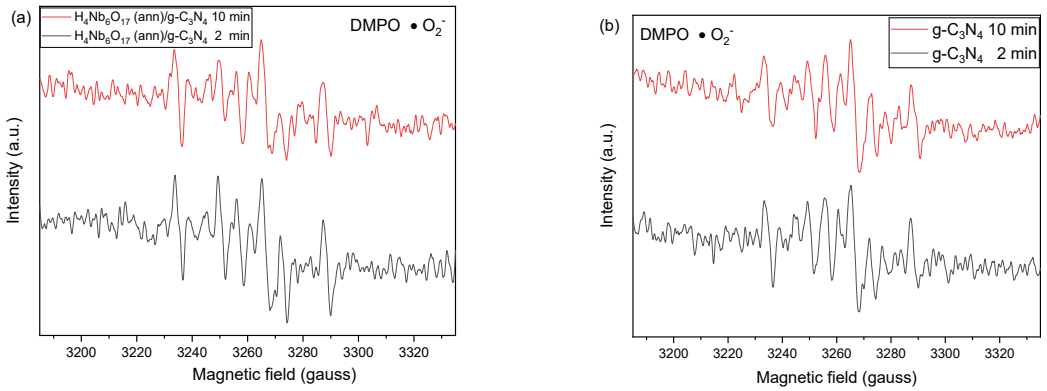

Figure S10. EPR spectra of $\cdot O_2^-$ radicals with irradiation for 2 min in methanol.

ESI Section 2: Composite optimization

XRD:

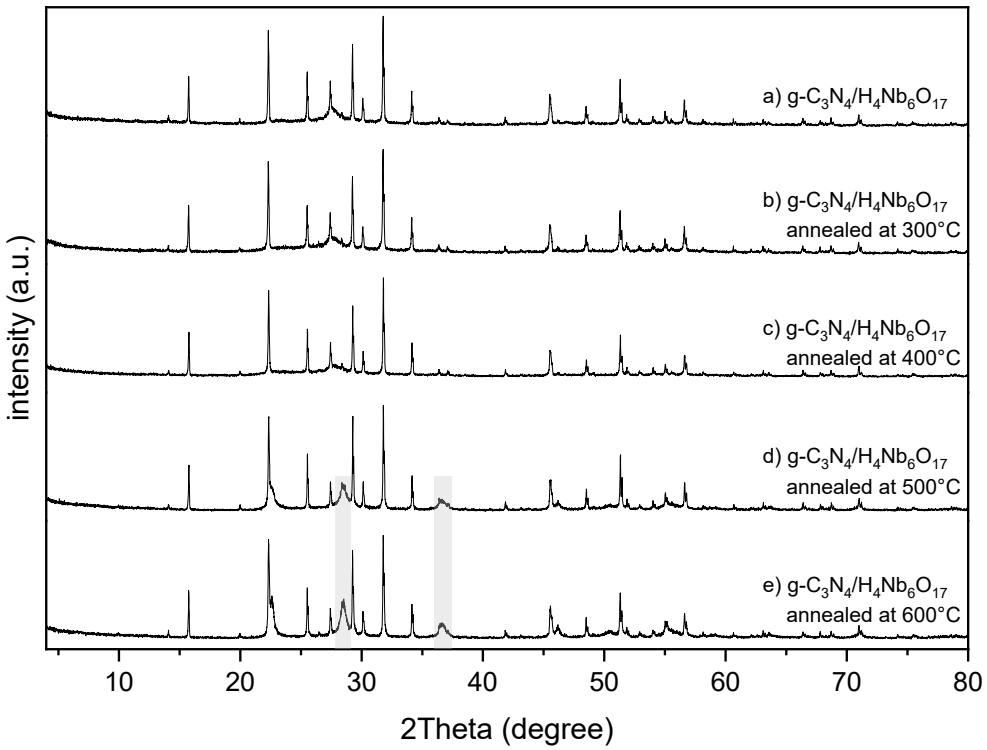

Figure S11. XRD patterns of g-C_3N_4/$H_4Nb_6O_{17}$ composites (a) before and after annealing at (b) 300°C, (c) 400°C, (d) 500°C and (e) 600°C.

When surveying the diffraction pattern of g-C_3N_4/$H_4Nb_6O_{17}$ (1:2) composite, it was found that the diffraction peaks were mostly ascribed to the crystalline structure of exfoliated $H_4Nb_6O_{17}$

(Figure S11 a). The failure in observing the characteristic peaks of g-C_3N_4 can be justified by the relatively lower degree of crystallinity and lower content of g-C_3N_4 in the mass ratio under study. However, crystallographic analyses proved to be useful in investigating the impact of the annealing treatment, carried out to potentially induce useful chemo-physical alterations (Figure S11 b-e). The diffraction peaks of the composite were preserved in the annealed samples, indicating that annealing at temperatures in the range between 300°C to 600°C did not destroy the g-C_3N_4/$H_4Nb_6O_{17}$ heterostructure. Moreover, higher annealing temperatures (above 500°C) were responsible for the detection of two new peaks at around 28.5° and 36.5°, which could be ascribed to a considerable physical change.

FTIR and UV-Vis:

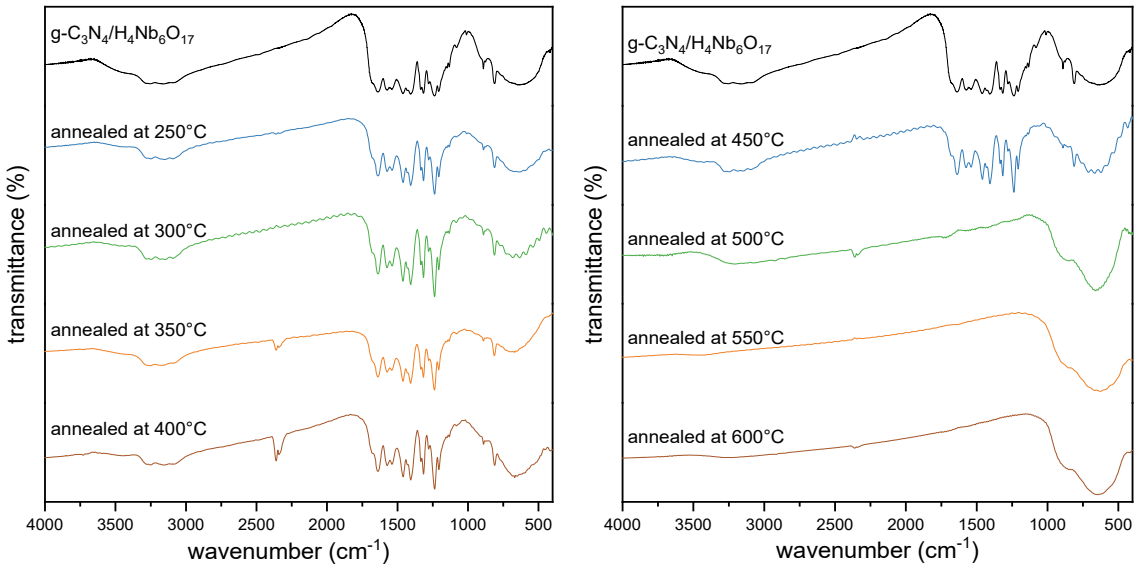

Figure S12. IR spectra of the composite annealed at different temperatures.

The samples annealed at temperatures between 250°C and 450°C share the same spectrum of the pre-annealed composite without any distinct dissimilarities, as shown in Figure S12. Meanwhile, in the spectra of the samples annealed at temperatures above 500°C, the characteristic bands of g-C_3N_4 are missing. This can be explained by the inferior thermal stability of g-C_3N_4, and $H_4Nb_6O_{17}$ dominating the physical features and properties of the composite. The sudden alteration in the compositional proportions is consistent with the conclusions drawn from the previous XRD.

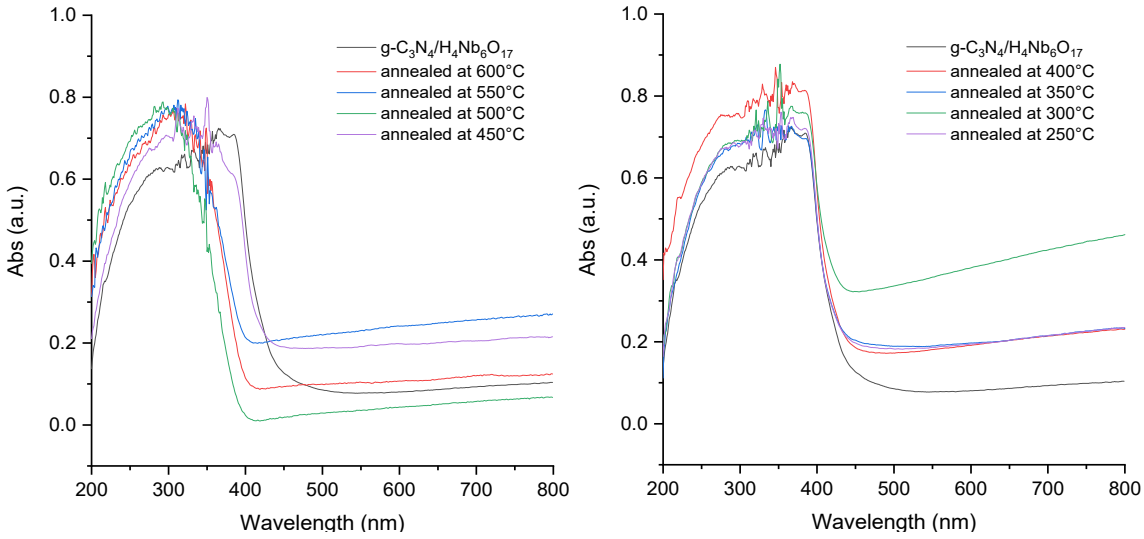

Figure S13. UV-vis spectra of $H_4Nb_6O_{17}$ annealed at different temperatures.

In Figure S13, the UV-vis spectra of the annealed composites suggest that a heating treatment within 450°C does not affect the optical properties of the material. However, above 500°C the absorption edge shifts towards shorter wavelengths closer to the pristine $H_4Nb_6O_{17}$. As supported by TEM images, the phenomenon observed is connected to the quantum confinement effect, in which a decrease in the nanoparticle size leads to wider bandgaps.

TEM:

From the TEM images in Figure S14, we can see the effect of heating on the composite, particularly that higher annealing temperatures above 500°C fractionate the composite structure, causing the decreasing aggregation and particle size. This is particularly noticeable at 600°C, for which particle size drops up to a diameter of approximately 22 nm. The amorphous shadowed areas ascribed to g-C_3N_4 are also harder to locate, suggesting a pronounced alteration of the ratio of substances in the overall chemical composition.

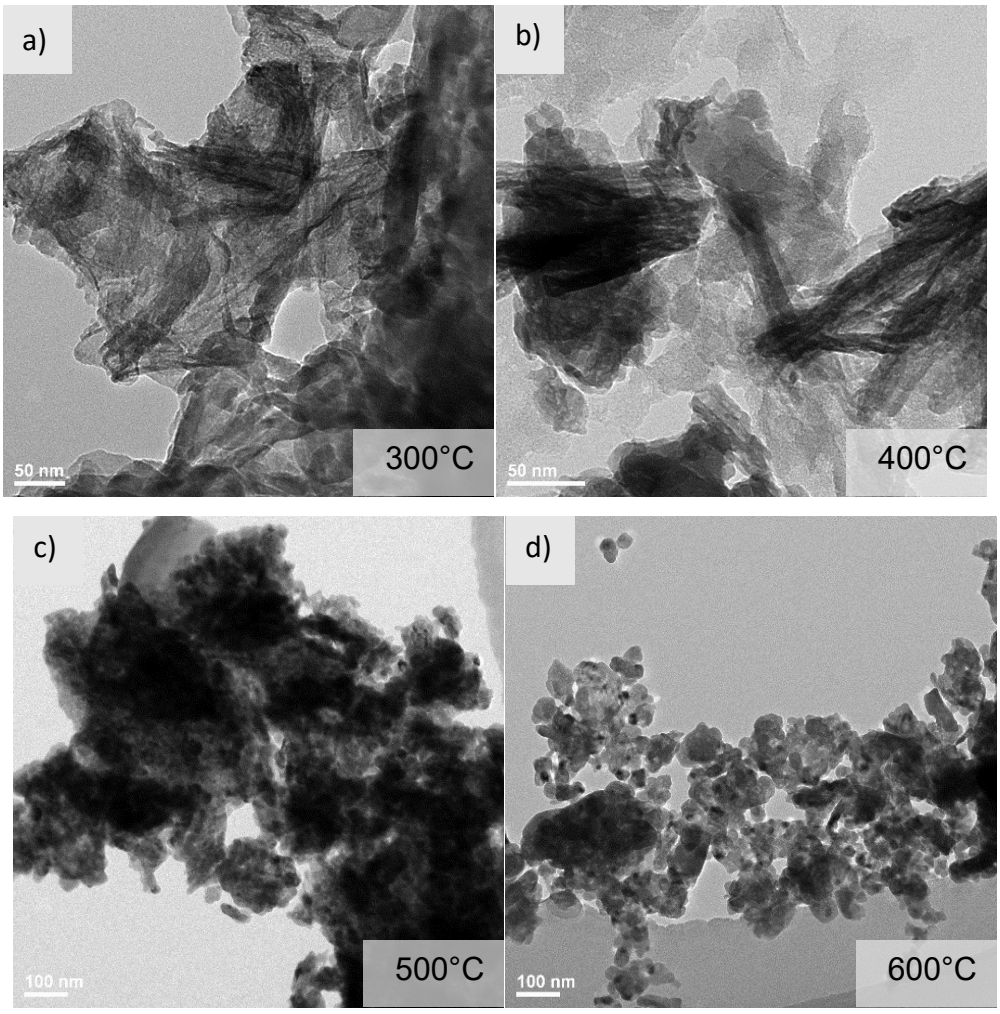

Figure S14. TEM images of the g-C_3N_4/$H_4Nb_6O_{17}$ composite annealed at (a) 300°C, (b) 400°C, (c) 500°C and (d) 600°C